Focus measurement with a simple pattern design

Chin-Yu Ku, Tan Fu Lei, and Hwang-Kuen Lin

The increasingly smaller depth of focus of advanced lithographic tools requires that the position of best focus be determined to ensure accuracy and efficiency. We present what we believe is a novel bar in bar that is drawn on a conventional chrome binary mask to translate focal errors into center-to-center shifts of outer and inner bars. An overlay measurement tool can easily measure this shift. A symmetrical center-to-center shift against best focus is created during defocus, and this shift can be well fitted by a second-order polynomial equation. Simply differentiating the fitted equation leads to an accurate and reliable focus value, with a maximum error of less than 0.05 μm. The proposed technique can also be employed to evaluate the tilt, field curvature, and astigmatism of advanced lithographic tools. © 2001 Optical Society of America

OCIS codes: 110.3960, 120.0120.

1. Introduction

To print smaller features in greater detail, advanced lithographic tools have reduced the wavelength from *G* line to *I* line to deep UV and increased the numerical aperture (NA) from 0.17 to 0.63 and larger. However, the Rayleigh depth of focus (DOF), DOF = $\pm\lambda/(2NA^2)$, has become smaller with technology advances. In light of the decreasing DOF, i.e., normally smaller than 1 μm, of modern small wavelength and high-NA lithographic tools, the position of best focus must be determined accurately and efficiently.

Many techniques have been developed to measure the best focus for steppers and scanners.[1–9] One technique for monitoring the best focus uses focal dot arrays to create patterns that can be read by the naked eye.[1] The small dots (opaque area) are drawn on the test reticle. The dot focus peaks are obtained by means of exposing the test reticle in a matrix form of varying energy and focus. As the energy increases, the focus dots will clear out at the extreme focus positions, leaving only the middle section. This middle section will continue to decrease as the energy increases. This process forms a peak, and the tip of the peak is the best focus. However, this method is somewhat less quantitative and is inadequate for advanced lithographic tools. Another conventional means of determining the best focus involves exposing a focus exposure matrix (FEM) wafer, where each exposure field uses a different focus and energy offset. After the wafer is developed, the best focus can be revealed at the selected energy by a scanning electron microscope (SEM). However, recent progress in photoresist has made it difficult to determine the best focus by SEM measurement of photoresist linewidth, because photoresist maintains nearly the same linewidth over a wide range of defocus. Terasawa *et al*. indicated that phase-shift angle errors at the mask could incur focal shifts of the aerial image of a contact hole.[10] Related investigations have noted the ability of the phase-shifting mask[11] to measure the best focus efficiently by employment of an overlay measurement system.[2,5] However, this technique is difficult to construct in the laboratory when a commercialized focus monitor mask is used. This procedural failure may be attributed to the complicated nature of the phase-shifting-mask process, which is sensitive to machine settings, to photoresist processing conditions, and to phase-shifting angle variations during mask making.[4] Line-end-shortening variation, which is caused by the nature of light diffraction, induces the rounding and the shortening at the end of photoresist line pattern. It has been reported that the change of the line length is changed to a varying focus. A previous study has indicated that best focus can be measured with this effect.[5] Moreover, despite the develop-

C.-Y. Ku and T. F. Lei (tflei@cc.nctu.edu.tw) are with the Department of Electronics Engineering and Institute of Electronics, National Chiao Tung University, 1001 Ta Hsueh Road, Hsinchu 300, Taiwan. H.-K. Lin is with the Vanguard International Semiconductor Corporation, Science-Based Industrial Park, Hsinchu 300, Taiwan.

Received 9 May 2000; revised manuscript received 8 February 2001.

0003-6935/01/162662-08$15.00/0

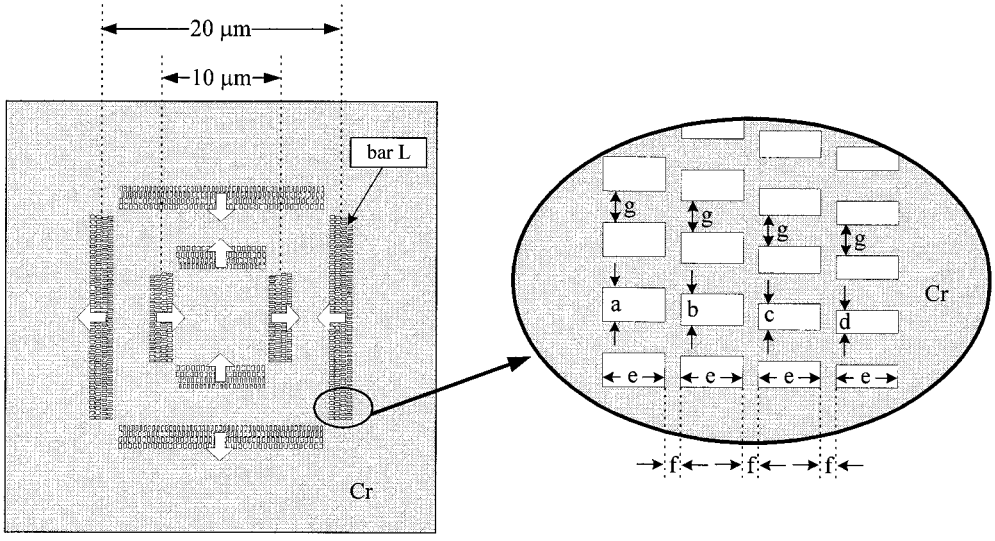

Fig. 1. Binary mask patterns for focus measurement.

ment of a focal monitor method using the line-end-shortening effect to measure the best focus, the experimental results show that the error of focal determination is approximately 0.1–0.2 μm.[6] Therefore this method is inaccurate for the best-focus determination of advanced lithographic tools.

This study describes what we believe is a novel means of measuring the best focus with a specially designed bar-in-bar (BIB) pattern. The inner and the outer bars are drawn on the same conventional chrome binary mask and printed simultaneously to translate focal errors into easily measurable overlay shifts. The information stored in the in-line resist patterns can sensitively reflect the actual image profile of the lithographic tools. The BIB resist patterns can be conveniently measured by the off-line overlay measurement system, which is normally used to monitor the overlay error between two different process layers, after development of the exposed wafer. A second-order polynomial equation can be used to characterize the center-to-center shift (termed hereafter as overlay shift) of the outer and the inner bars under various focal settings. The adjacent inner and outer bars are mirrored to each other to create the overlay shift when the wafer moves away from the best-focus position. Simply differentiating the fitting equation allows for accurate and reliable determination of the best focus. This technique can also be employed to monitor the tilt, field curvature, and astigmatism of advanced lithographic tools.

2. Theory

Owing to the diffraction of light, the shrinkage percentages of various contact hole sizes markedly differ when the wafer moves away from the best focus (a state generally referred to as being defocused). In this study a novel BIB pattern is used to measure the best focus on the basis of the shrinkage performance of contact holes. Figure 1 illustrates the specially designed BIB pattern layout, which is drawn on a binary mask. Each bar of the pattern comprises four columns of contact holes, which have the same length (e = 0.4 μm) but different spaces (f, g) and widths (a–d) on each column. During the defocus the gravity center of the bar shifts, owing to the varying size changes of the contact holes. Four columns of gradually changed contact holes are used to create a smoother intensity profile. Table 1 presents a split table of different sizes a–d, f, and g as shown in Fig. 1 to yield the best performance. Various pattern sizes are first printed by a deep-UV stepper and then measured by an overlay measurement tool. Notably, the exposure energy dependency is also considered during selection of the pattern size combination. Figure 2 displays the SEM

Table 1. Split Conditions of the Novel BIB Pattern[a]

	Split Table of Different Contact Hole Sizes (a–d) and Seperations (f, g)									
	Type 1	Type 2	Type 3	Type 4	Type 5	Type 6	Type 7	Type 8	Type 9	Type 10
a	0.4	0.3	0.22	0.35	0.25	0.4	0.3	0.22	0.35	0.25
b	0.35	0.25	0.2	0.3	0.22	0.35	0.25	0.2	0.3	0.22
c	0.3	0.22	0.17	0.25	0.2	0.3	0.22	0.17	0.25	0.2
d	0.25	0.2	0.15	0.22	0.17	0.25	0.2	0.15	0.22	0.17
f	0.1	0.1	0.1	0.2	0.2	0.1	0.1	0.1	0.2	0.2
g	0.1	0.1	0.1	0.1	0.1	0.2	0.2	0.2	0.2	0.2

[a]Refer to Fig. 1.

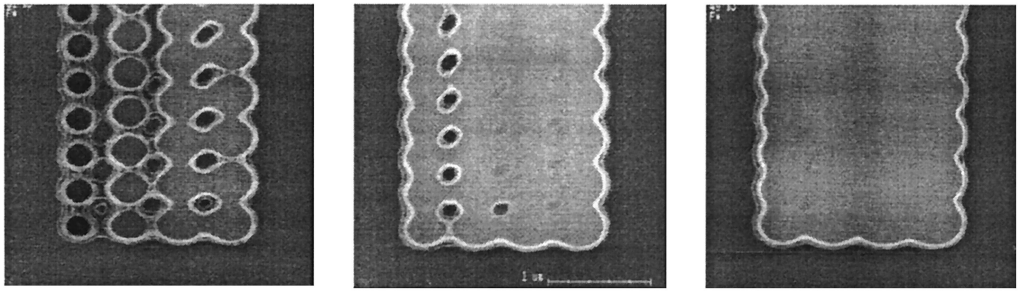

Fig. 2. SEM pictures of different levels of energy: (a) 31 mJ/cm^2, (b) 40 mJ/cm^2, (c) 49 mJ/cm^2.

pictures of different levels of energies at best focus (type 8). The residual photoresist between holes induces a measurement error and reduces the stability. Therefore, in this study, the energy is selected to be approximately four times the energy to clear, E_0 ($E_0 \sim$ 12 mJ/cm^2), i.e., the minimum required energy to remove a nonpatterned photoresist, to overexpose the resist. In addition, the dose to size for a 0.2-μm dense line pattern is ~20 mJ/cm^2.

Figure 3 illustrates the horizontal (x-direction) overlay shift of the BIB for various split conditions. These figures reveal symmetrical overlay shifts when the wafer moves away from the best focus in positive and negative directions. For accurate determination of the best focus, a second-order polynomial equation is used to fit the overlay shift. A conventional software tool, such as Microsoft Excel, can be employed to verify the fitting results. Herein the R-squared value is used to confirm the validity of the second-order polynomial equation. The data points can be easily fitted with an R-squared value exceeding 0.98 when the contact hole parameters a, b, c, d, f, and g are 0.22, 0.20, 0.17, 0.15, 0.10, and 0.20 μm (type 8), respectively. This combination is used for the following discussion and application.

Figure 4 illustrates the overlay shift of various exposure energies under different focus levels (type 8). Although a low energy benefits from a large overlay shift and high focus sensitivity, two disadvantages are the measurement noise mentioned above and the larger fitting error of the polynomial equation. In this example the energy 49 mJ/cm^2 is selected to eliminate these two problems. Figure 4 also shows a second-order polynomial fitting curve to illustrate the correlation between experimental and fitted results. Furthermore, a modeling program PROLITH/2 is implemented to verify the resist pattern performance. According to our results, large and small patterns obviously differ in terms of the deformations of the latent image profile. Figure 5 summarizes the lithographic performance and simulation results on a negative-direction focal shift, because our results suggest that the overlay shift is symmetrical to the best focus of the exposure tool, owing to the symmetrical behavior of resist patterns in positive and negative focused shifts. In addition, the small concavities discovered on the edge of the resist patterns around the best-focus region correlate with the simulation results. However, the small concavities do not distort the overall measurement results, because the overlay measurement tools take the center of gravity for each bar.

To elucidate the BIB behavior under defocus, a SEM is used to measure the linewidths and the space widths. Figure 6 displays the measurement methodology as explained in the following. Experimental results indicate that the bar width (space width) obviously becomes larger under defocus when the exposure energy is set to 49 mJ/cm^2. To confirm the BIB

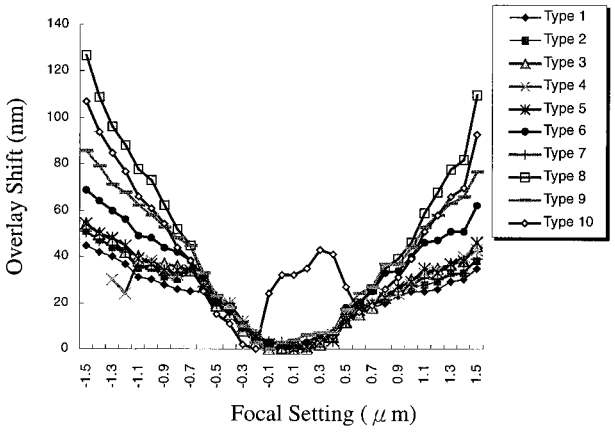

Fig. 3. Overlay shift of BIB pattern for various split conditions.

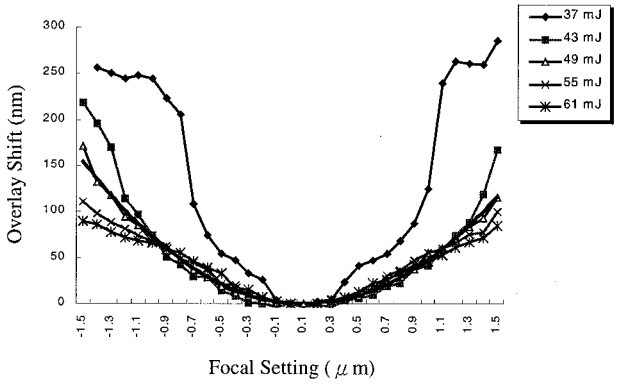

Fig. 4. Overlay shift of various exposure energy (type 8).

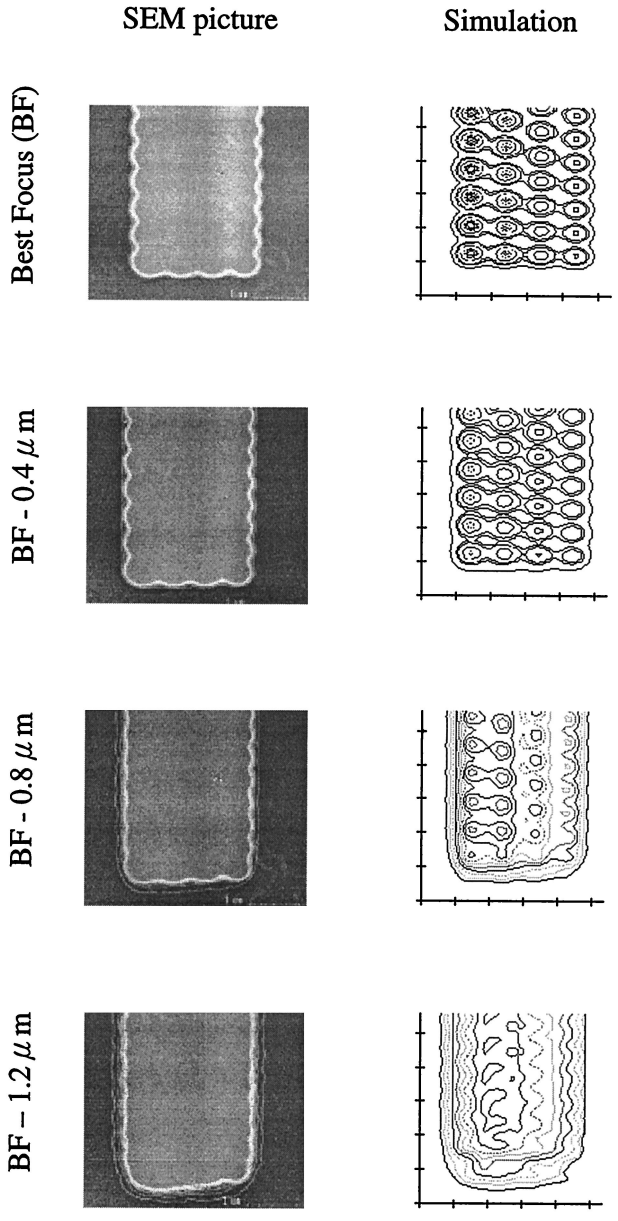

Fig. 5. Lithographic performance and simulation result.

pattern behavior by SEM, the following assumptions are made. L_1 and L_2 are the linewidths between inner and outer bars under best focus and defocus, respectively. The space widths S_1 and S_2 represent the space widths of the inner bar under best focus and defocus. In addition, u and v are the outward shifting of the boundary of large and small holes, respectively, when the focus is shifted away from best focus. Therefore the shifts u and v can be represented by

$$u = (L_1 - L_2)/2, \qquad \text{boundary shift of large holes;} \tag{1}$$

$$v = S_2 - S_1 - u, \qquad \text{boundary shift of small holes.} \tag{2}$$

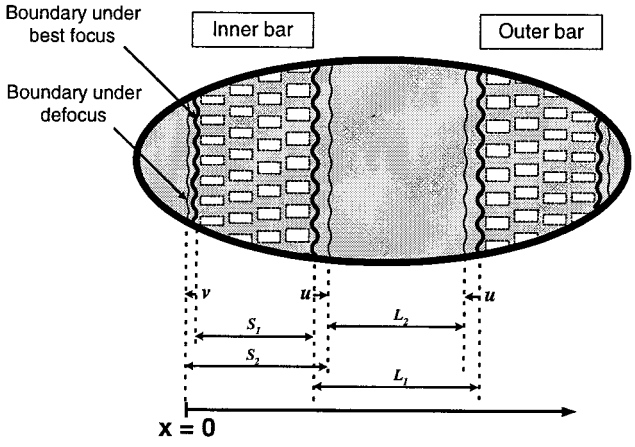

Fig. 6. BIB overlay shift measured by SEM methodology.

The center positions of the inner bar under best focus and defocus are

$$x_{\text{BestFocus}} = v + S_1/2, \tag{3}$$

$$x_{\text{Defocus}} = S_2/2. \tag{4}$$

Therefore the center position shift of the inner bar under defocus can be obtained by subtraction of Eq. (3) from Eq. (4). The shift can be represented by

$$\Delta x = x_{\text{BestFocus}} - x_{\text{Defocus}} = \frac{S_2}{2} - \left(v + \frac{S_1}{2}\right)$$

$$= \frac{1}{2}(S_2 - S_1) - v = \frac{u - v}{2}. \tag{5}$$

The fact that the shifts of inner and outer bar center have the same magnitude but opposite direction accounts for why the overlay shift is twice that of the inner bar shift (the shift directions are also shown in Fig. 1). Thus the measured overlay shift is $(u - v)$. The above derivation reveals that the overlay shift can be obtained by the SEM measurement of the linewidths L_1, L_2 and the space widths S_1, S_2. Therefore the overlay shift can be represented by

$$u - v = u - (S_2 - S_1 - u)$$

$$= 2u + (S_1 - S_2)$$

$$= (L_1 - L_2) + (S_1 - S_2). \tag{6}$$

Figure 7 illustrates the boundary shifts (measured by SEM) of large and small holes u and v for various exposure energies. According to this figure, the shift of the large holes increases with the defocus value, and the shift of small holes remains almost a constant under the previous selected energy (49 mJ/cm^2). Subtracting the u by v can produce the overlay shift $(u - v)$, as depicted in Fig. 8 (SEM measurement). Moreover, the measurement results of the overlay measurement tool (overlay shift) and of the SEM correlate well with each other.

To further verify the overlay shift under defocus, the aerial image of the bar is investigated to deter-

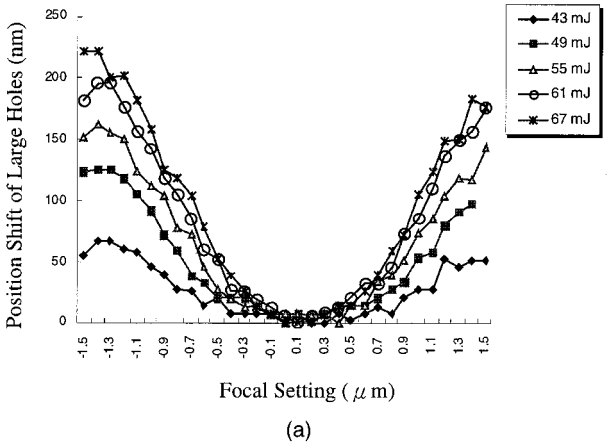

(a)

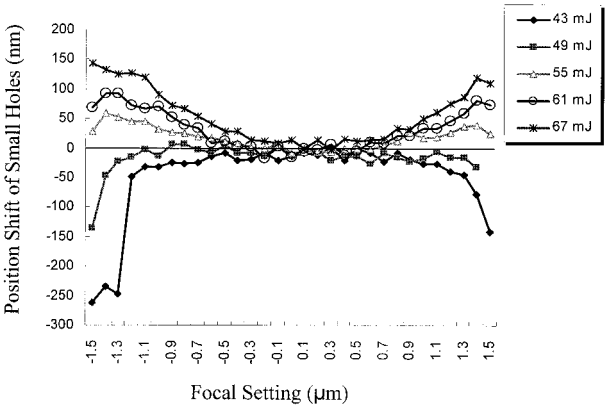

(b)

Fig. 7. Boundary shift of (a) large holes u and (b) small holes v (measured by SEM).

mine the width and the position of each bar by means of taking the average intensity along with the bar. Figure 9 illustrates the average intensity for different defocus values. The previous SEM measurements revealed that the boundary between developed and nondeveloped regions of the 0.15-μm-wide side (small holes) remains nearly at the same position under

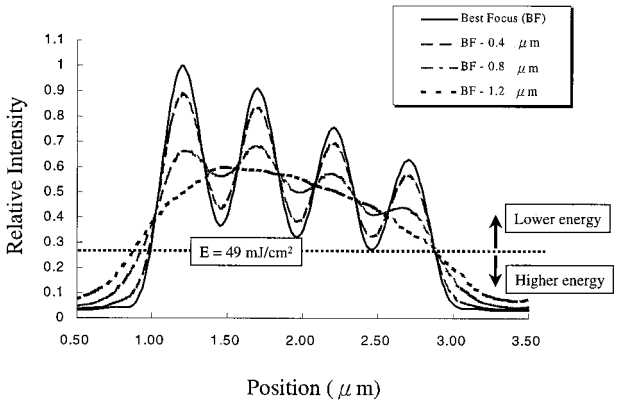

Fig. 9. Average aerial intensities of the BIB bar.

defocus when the exposure energy is 49 mJ/cm^2. The dashed curve in Fig. 9 represents the level of the optimized energy (49 mJ/cm^2) to achieve the zero shift on the 0.15-μm-wide side. When the wafer is moved away from the best focus in either positive or negative directions, the aerial image of each contact hole becomes blurred, and distinguishing between each hole is more difficult. A single image profile occurs when the defocus value exceeds 1.2 μm, owing to the diffraction of light. Notably, the width and center position of the bar can be calculated from the intensity distribution displayed in Fig. 9. Therefore the overlay shift under defocus is obtained and depicted in Fig. 8 [simulation (PROLITH/2)]. The close correlation between different measurements and simulation results confirms the experimental setup again.

From the previous derivation and verification, a reliable curve can be obtained by fitting of the measured overlay shift with a second-order polynomial equation. Because the overlay shift is symmetrical with respect to best focus, we can obtain the value of the best focus by taking the derivative (displayed in Fig. 10) of the fitting curve, and the best focus is located at the point where the derivative is zero.

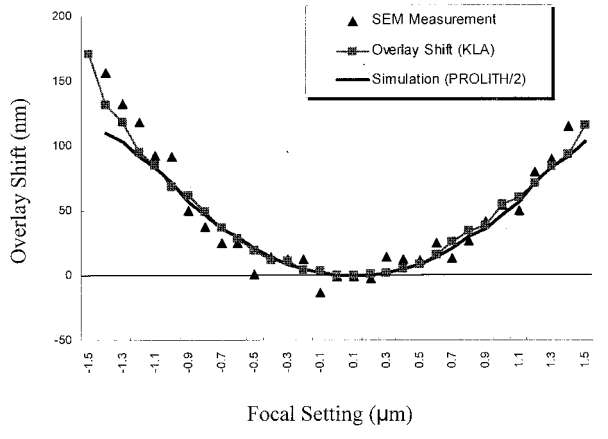

Fig. 8. Overlay shift obtained from SEM, overlay measurement system (KLA), and simulation (PROLITH/2).

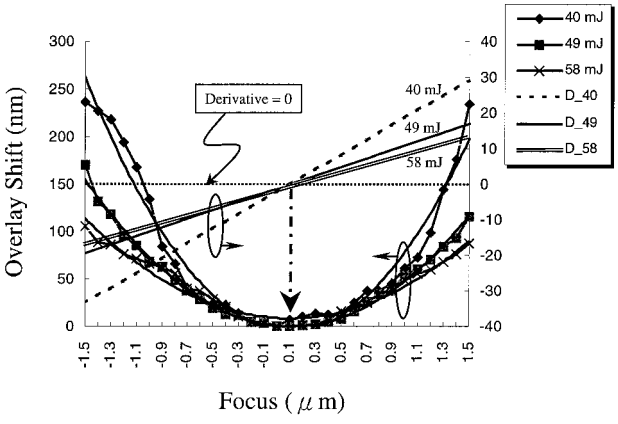

Fig. 10. Fitting curves and derivative results of three energy levels.

Table 2. Sampling Plan for 0.4-μm Focus Step

	Plan 1	Plan 2	Plan 3	Plan 4	Plan 5	Plan 6	Plan 7
Focus setting (μm)	−1.5	−1.4	−1.3	−1.2	−1.1	−1	−0.9
	−1.1	−1	−0.9	−0.8	−0.7	−0.6	−0.5
	−0.7	−0.6	−0.5	−0.4	−0.3	−0.2	−0.1
	−0.3	−0.2	−0.1	0	0.1	0.2	0.3
	0.1	0.2	0.3	0.4	0.5	0.6	0.7
	0.5	0.6	0.7	0.8	0.9	1	1.1
	0.9	1	1.1	1.2	1.3	1.4	1.5
Total points	7	7	7	7	7	7	7

3. Experiment

The resist was coated onto silicon substrates that were hexamethyl-disilazane-vapor primed. The positive deep-UV resist was spin coated to 0.7-μm thickness and prebaked at 110 °C for 90 s. All patterns were exposed by a KrF excimer laser stepper with a 0.57-NA lens, and the postexposure bake was performed at 110 °C for 90 s. The resist films were developed in a 2.38 wt.% tetramethylammonium-hydroxide-based developer for 60 s. The overlay shift was measured by a metrology tool KLA Model 5200, which is designed to measure the overlay error between two different process layers, such as active layer and polygate. A Hitachi Model S-9200 SEM is used to measure the linewidths and the space widths of the resist pattern to confirm the measured overlay results. Here the optimized exposure energy is selected to be approximately four times that of the energy to clear, E_0, to yield the best performance.

4. Results and Discussion

Figure 10 illustrates the overlay shift and derivative of the fitting curves for three energy levels, 40, 49, and 58 mJ/cm^2. The best focuses determined by these three conditions are 0.103, 0.104, and 0.095 μm, and they are nearly the same. Therefore, according to our results, the novel BIB can determine the best focus over a wide range of energy levels.

The FEM of five different central focus settings, −0.2, −0.1, 0, 0.1, and 0.2 μm, is employed to verify the accuracy and the stability of the BIB pattern. The focal step of the FEM was 0.1 μm, and the total number of defocused settings is 31. For example, if the central focus setting is 0 μm, the defocused setting ranges include −1.5, −1.4, −1.3, . . . , −0.1, 0 (central focus), 0.1, . . . , 1.3, 1.4, 1.5 μm, and the total focus setting is 31. If the central focus setting is −0.2 μm, the defocused values range from −1.7 to 1.3 μm. On the basis of our discussion above on exposure energy, the energy is fixed to 49 mJ/cm^2, and the energy step is 0. For each central focus setting ten sets of data are obtained. Therefore 50 FEMs are exposed and separated into five different central focus settings to confirm the validity of the experimental procedure. The overlay shifts of 31 defocused BIB patterns for a specific central focus setting are measured to determine the best focus value. After the fitting procedure of these shift data, the best focus can be obtained at the position where the derivative is zero.

Two problems will exist if this BIB pattern is implemented on production lines: First, the collected data points may not cover both sides of the fitting curve or provide adequate information to accurately determine the best focus. Restated, if the best focus is not located at the center of the 31 defocused setting, whether or not the BIB method can still accurately determine the best focus must be addressed. The second problem involves using the previously described 31 defocused BIB patterns to determine the best focus. This is time consuming when the best-focus values within an exposure field, such as tilting and field curvature, are of interest. To solve the previous two problems, different data sampling plans based on the 50 FEMs data are verified to attain the solution. The sampling plan starts from the 0.2-μm focus step and reduces the data points from 31 to 15. According to our results, 15 measurement points with 0.2-μm focus steps can accurately determine the best focus. Therefore the focal step extends to 0.3, 0.4, and 0.5 μm, and the sampling points reduce to 9, 7, and 5 points, respectively. During the verification procedure, different starting focal values are verified. For example, in the 0.4-μm focus step, the starting sampling point can be −1.5, −1.4, −1.3, −1.2, −1.1, −1.0, or −0.9 μm. Table 2 lists the measured focus settings for a 0.4-μm focus step. Figure 11 displays the measured best-focus values (in the x direction) of plan 1, based on a 0.4-μm focus step. Comparing the focal setting of the exposure tool and the BIB-measured result reveals that the maximum error among the 50 best-focus results is obtained, with an error less than 0.05 μm. This error almost reaches the limit of the exposure tool's focus control capability. Notably, the errors are also smaller than 0.05 μm for plans 2–7. Therefore we conclude that an accurate and efficient focus determination method has been provided with an error less than 0.05 μm when the following two criteria are satisfied. First, a minimum of seven measurement points with a focal

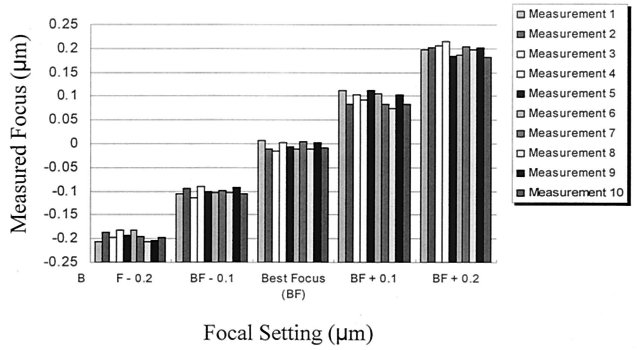

Fig. 11. Measured focus value (plan 1) for five different central focus settings.

step of 0.4 μm are required. Second, at least three points among the measured overlay results must be located on either positive or negative defocus regions. Thus the best focus should be located within the ±0.4-μm range of the initial central focus setting of the FEM. Fortunately, the daily focus drift is small, and the field curvature is normally less than 0.3 μm for advanced exposure tools. Therefore this sampling plan is adequate for routinely monitoring the best focus over the entire exposure field.

With the novel BIB the field curvature can be obtained if more focus values are determined within the exposure field. Figure 12 illustrates the three-dimensional view of an exposure field (21 mm × 21 mm) based on 21 × 21 measurement points. The focus difference in the exposure field is 0.29 μm, and the maximum and the minimum focus values are 0.16 and −0.13 μm, respectively. Evidently, a tilt error exists in the field, and it can be corrected by the leveling system of the exposure tool. The best focus of an exposure tool is normally measured daily to monitor the machine status for mass production. However, the tilt of the exposure field is measured on a weekly or a monthly basis, because of the time-consuming nature or the limitations of focal measurement methodology. Notably, the best focus on four corners of the exposure field should be obtained to determine the tilt. By use of the novel BIB pattern, seven defocus overlay shifts are sufficient for one focus determination. Therefore the tilting can be easily determined from all 28 measurement results. An advantage of the BIB method is that the focus and the tilt results can be obtained by an off-line overlay measurement system. The exposure tool can still be run for production during the focus determination and, therefore, increase the availability of the exposure tool. As is well known, the tilt monitor method becomes increasingly important, owing to the decreasing DOF of advanced exposure tools and processes. The BIB pattern proposed in this study can monitor the tilt of an exposure tool on a daily basis. Furthermore, the astigmatism, i.e., the best-focus difference in the x and the y directions, can be easily obtained by subtraction of the best focus in x from the best focus in y.

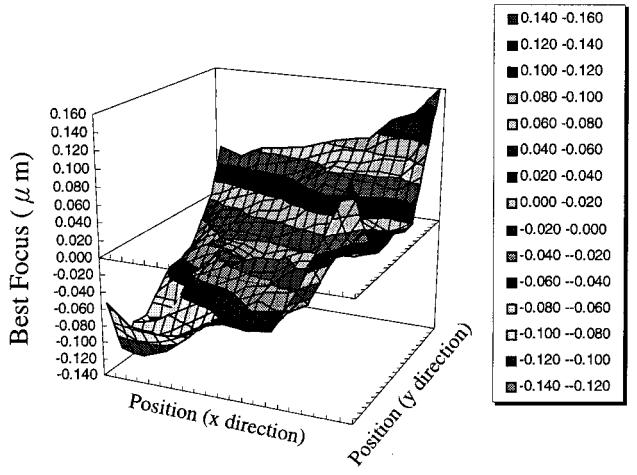

Fig. 12. Three-dimensional view of an exposure field (21 mm × 21 mm).

5. Summary

In this study we have presented a modified bar-in-bar pattern (BIB), which is drawn on a conventional chrome binary mask, for accurate and efficient determination of the best focus. The good correlation between the overlay shift, simulation results, and SEM measurements demonstrates the effectiveness of the proposed method. A seven-point sampling plan is also developed for efficient determination of the best focus with an error smaller than 0.05 μm. The proposed method can also be applied to determine the tilting and field curvature of the exposure field.

The authors thank the National Science Council of China for financially supporting this research under contract NSC 88-2215-E009-045.

References

1. S. Stalnaker, P. Luehrmann, and J. Waelpoel, "Focal plane determination for sub-half micron optical steppers," Microelectron. Eng. **21,** 33–43 (1993).
2. T. A. Brunner, A. L. Martin, R. M. Martino, C. P. Ausschnitt, T. H. Newman, and M. S. Hibbs, "Quantitative stepper metrology using the focus monitor test mask," in *Optical/Laser Microlighography VII*, T. A. Brunner, ed., Proc. SPIE **2197,** 541–549 (1994).
3. W. H. Arnold, E. Barouch, U. Hollerbach, and S. A. Orszag, "A focus vernier for optical lithography," in *Integrated Circuit Metrology, Inspection, and Process Control VII*, M. T. Postek, ed., Proc. SPIE **1926,** 380–392 (1993).
4. A. D. Katnani and B. J. Lin, "Phase and transmission error study for the alternating element (Levenson) phase-shifting mask," in *Optical/Laser Microlithography V*, J. D. Cuthbert, ed., Proc. SPIE **1674,** 264–270 (1992).
5. K. Suwa, H. Tateno, N. Irie, and S. Hirukawa, "Automatic laser scanning focus detection method using printed focus pattern," in *Optical/Laser Microlithography VIII*, T. A. Brunner, ed., Proc. SPIE **2440,** 712–720 (1995).
6. Y. C. Kim, G. S. Yeo, J. H. Lee, H. Kim, and U. I. Chung, "Automatic in-situ focus monitor using line shortening effect," in *Metrology, Inspection, and Process Control for Microlithography XIII*, B. Singh, ed., Proc. SPIE **3677,** 184–193 (1999).

7. T. A. Brunner, S. Cheng, and A. E. Norton, "A stepper image monitor for precise setup and characterization," in *Fiber Optics Reliability: Benign and Adverse Environments II*, R. A. Greenwell, D. K. Paul, and S. G. Wadekar, eds., Proc. SPIE **922,** 366–375 (1988).
8. T. A. Brunner, J. Lewis, and M. Manny, "Stepper self-metrology using automated techniques," in *Optical Fibers in Medicine V*, A. Katzir, ed., Proc. SPIE **1201,** 286–297 (1990).
9. M. van den Brink, H. Franken, S. Wittekoek, and T. Fahner, "Automatic on-line wafer stepper calibration system," in *Integrated Circuit Metrology, Inspection, and Process Control IV*, W. H. Arnold, ed., Proc. SPIE **1261,** 298–314 (1990).
10. T. Terasawa, N. Hasegawa, T. Kurosaki, and T. Tanaka, "0.3 μm optical lithography using a phase-shifting mask," in *Optical/Laser Microlithography II*, B. J. Lin, ed., Proc. SPIE **1088,** 25–33 (1989).
11. M. D. Levenson, N. S. Viswanathan, and R. A. Simpson, "Improving resolution in photolithography with a phase-shifting mask," IEEE Trans. Electron Devices **ED-29,** 1828–1836 (1982).